*Entropy* **2015**, *17*, 866-881; doi:10.3390/e17020866

OPEN ACCESS

*entropy*

**ISSN 1099-4300**

www.mdpi.com/journal/entropy

*Article*

# Optimal Design of Magnetohydrodynamic Mixed Convection Flow in a Vertical Channel with Slip Boundary Conditions and Thermal Radiation Effects by Using an Entropy Generation Minimization Method

**Mohamad Yaghoub Abdollahzadeh Jamalabadi [1,2], Jae Hyun Park [3,*] and Chang Yeop Lee [4]**

1. Ship Engineering Department, School of Mechanical Engineering, Maritime University of Chabahar, Chabahar 99717-56499, Iran; E-Mail: muhammad_yaghoob@yahoo.com
2. Graduate School of Mechanical and Aerospace Engineering, Gyeongsang National University, Jinju, Gyeongnam 660-701, Korea
3. Department of Aerospace and Software Engineering and Research Center for Aircraft Parts Technology, Gyeongsang National University, Jinju, Gyeongnam 660-701, Korea
4. Thermochemical Energy System R&BD Group, Korea Institute of Industrial Technology, Cheonan-si, Chungcheongnam-do 331-822, Korea; E-Mail: cylee@kitech.re.kr

* Author to whom correspondence should be addressed; E-Mail: parkj@gnu.ac.kr; Tel.: +82-55-772-1585; Fax: +82-55-772-1580.

Academic Editor: Kevin H. Knuth

*Received: 18 November 2014 / Accepted: 5 February 2015 / Published: 13 February 2015*

---

**Abstract:** Investigation of the effect of thermal radiation on a fully developed magnetohydrodynamic (MHD) convective flow of a Newtonian, incompressible and electrically conducting fluid in a vertical microchannel bounded by two infinite vertical parallel plates with constant temperature walls through a lateral magnetic field of uniform strength is presented. The Rosseland model for the conduction radiation heat transfer in an absorbing medium and two plates with slip-flow and no-slip conditions are assumed. In addition, the induced magnetic field is neglected due to the assumption of a small magnetic Reynolds number. The non-dimensional governing equations are solved numerically using Runge–Kutta–Fehlberg method with a shooting technique. The channel is optimized based on the Second Law of Thermodynamics by changing various parameters such as the thermal radiation parameter, the temperature parameter, Hartmann number, Grashof to Reynolds ratio, velocity slip length, and temperature jump.

**Keywords:** thermal radiation; slip boundary; mixed convection; entropy minimization; magnetohydrodynamic (MHD)

**PACS Codes:** 05.70.-a ; 44.40.+a ; 47.55.pb; 47.35.Tv; 47.65.-d; 83.50.Lh

---

## 1. Introduction

Heat transfer in free and mixed convection in vertical channels takes place in many applications such as the design of cooling systems for electronic devices [1], chemical processing equipment [2], microelectronic cooling [3], and solar energy [4], *etc.* There is some research that deals with the assessment of the temperature and velocity fields for the vertical fully developed flow without considering the effect of thermal radiation [5,6], but heat transfer by simultaneous radiation and convection is important in various cases including combustion flows [7], furnaces [8], high-temperature reactors [9] and heat exchangers [10], combustion [11], solar energy [12], thermal radiative loading [13], and many others [14–16]. In addition, the significance of radiative heat transfer is found in the industrial processes and magnetohydrodynamic (MHD) flow [17]. MHD is the field of fluid mechanics that deals with the dynamics of an electrically conducting fluid under the influence of a magnetic field. MHD has gained considerable importance because of its wide ranging applications in fluid flow control and propulsion [18,19].

Slip effects under boundary conditions and thermal radiation in the fluid is the topic of many researches [20]. Industrial application of this combination in microchannels is in the flow of metal vapors [21,22], plasma chemical vapor deposition (CVD) [23], electrohydrodynamic mixers [24], rhombus microchannels [25], and laser-driven radiative shock experiments [26]. As stated in common textbooks [27] the slip flow regime is valid when $0.01 \leq \mathrm{Kn} \leq 0.1$. In the slip flow regime the flow is dense enough to be considered a continuum but the no-slip boundary condition is not valid. In this regime a sub-layer on the order of one mean free path, known as the Knudsen layer, starts to become dominant between the bulk of the fluid and the wall surface. In the slip flow regime the flow is ruled by the Navier–Stokes equations, and rarefaction properties are simulated by the limited slip at the wall using Maxwell's velocity slip and von Smoluchowski's temperature jump boundary conditions. However the slip boundary condition is not limited to compressible fluid flow and as shown by experiments for common Newtonian liquids such as isopropanol, *n*-hexadecane, water, ethanol, and toluene in microchannels with heights of approximately 350 nm–5 μm, it is demonstrated that the behaviour is not the same as expected by the no-slip boundary condition, and the slip boundary condition should be applied [28].

When fluid flow is confined by small systems such as micro/nanochannels, some discontinuity in velocity and temperature profiles might happen at the interface of the fluid and solid surface [28–30]. Ulmanella and Ho [28] experimentally observed the velocity for various micro-sized channels, which is a function of shear rate, type of liquid and surface morphology. Bocquet and Barrat [29] described a possibility of temperature jump along with velocity slip. They modeled velocity slip and temperature jump by introducing velocity slip length and temperature slip length terms, respectively. The velocity slip and temperature jump relations should be used as the boundary conditions for liquid-solid interface of micro/nanosized channel in other references [27].

One of the potential applications of current research is the design of collectors for thermal storage [30], such as in thermo-syphon solar water heaters [31]. As shown in Figure 1, a vertical channel acting as a collector of the thermal energy contains a moving phase change material heated by the solar radiation. This kind of configuration is commonly found in solar collectors for thermal storage applications and thermo-syphon solar water heaters. The working fluid is forced by a pump to transfer thermal energy from the collector to the thermal storage tank. The designed pump should create enough pressure gradients through the channel to ensure stable movement of the phase change against the wall friction and the natural convection flow caused by temperature difference between two walls of the channel. Here the right wall is assumed to be at a higher temperature than the left wall because it is heated by solar radiation and the left wall, the cold heat source, is at the melting point of the phase change material. The purpose of a solar thermal collector is to absorb as much sunlight as possible and a number of studies have been focused on increasing the absorptivity of the fluid medium in the solar collector. Recently, researchers have found that the absorptivity can be significantly enhanced by using a nanofluid that is a mixture of liquid and suspended nanoparticles [32]. By seeding the nanoparticles in the base fluid, the extinction coefficient of the medium increases over 100 $cm^{-1}$ [32]. It is apparently an optically thick medium even for microchannels whose characteristic length is on the microscale and therefore the optically thick medium approximation is applicable to the analysis of radiative transfer. In addition for the application of metal gas vapors and plasma in microchannels [21–23] the radiative absorption coefficient of the medium is large enough to assume a thick optical medium. The radiative heat transfer through such media can be simplified by the Rosseland diffusion approximation [4]. Other than the other applications [33–39], the other trend of analysing flow and heat transfer is to apply a Second Law of Thermodynamics analysis, and its design-related concept of entropy generation minimization. Entropy generation is associated with thermodynamic irreversibility, which presents in all flow and heat transfer developments. Bejan [40,41] founded theoretical work on entropy generation in flow systems. He showed that by minimizing the entropy, the efficiency of a thermal system could be enhanced based on the Second Law of Thermodynamics. Thereafter, several authors [42–51] have analyzed different problems to study the entropy effects on thermal systems and to find ways to minimize them.

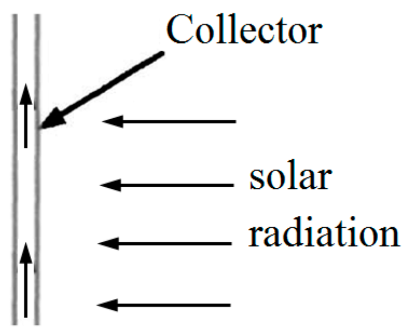


**Figure 1.** Thermal storage thermo-syphon solar water heaters.

Considering all the above, the goal of the current research was to optimize the steady state fully developed mixed convection incompressible flow in a vertical microchannel such that the walls of the channels are subjected to different wall temperatures and the Rosseland approximation model. The effects of thermal radiation coefficient, the thermal parameter, Prantdl number, Reynolds number, Hartmann number, Grashof number, Hartmann number, specific heat ratio and Knudsen number on entropy generation are investigated analytically.

## 2. Governing Equations

In order to understand the fundamental basics of the fully developed laminar flow through an infinitely long vertical channel, a simple configuration as shown in Figure 2 is considered. An optically thick incompressible fluid is confined by two parallel planar walls that are separated by a distance of 2L. The two infinite vertical parallel plates of the channel are non-permeable, but there are slip-flow conditions on both of the plates. Since the infinitely long geometry is assumed, the flow velocity u is only a function of the y-direction across the channel and the origin of the system is placed at the middle point. The left and right walls (y = ±L) are maintained at the uniform temperatures of $T_L$ and $T_R$, respectively. The temperature difference of the two plates is also assumed to be high enough to induce heat transfer due to radiation. A uniform magnetic field of strength B is applied perpendicular to the plates of the channel. The magnetic Reynolds number is presumed small enough consequently that the induced magnetic field is neglected. In the steady state, this system can be described by momentum and energy equations employing Boussinesq approximation for buoyancy force (All fluid properties are assumed to be constant except that of the influence of density variation with temperature is considered only in the body force term). By ignoring the horizontal component of the velocity in the continuity equation, the simplified momentum equation for fully developed velocity (u(y)) is:

$$\frac{d^2u}{dy^2}=\frac{1}{\mu}\frac{dp}{dx}+\frac{\sigma uB^2}{\mu}-\frac{\rho_0 g\beta\left(T-T_{ref}\right)}{\mu} \tag{1}$$

and the energy equation for thermal radiative absorbance of solar radiation in phase change material (radiative heat flux transport in a gray medium) is based on the Rosseland approximation (diffusion of radiative heat flux) which is useable when the medium is optically thick, and is recommended for use in problems where the optical thickness is greater than 3 [4]:

$$\frac{d^2T}{dy^2}=-\frac{4\sigma}{3k\chi}\frac{d^2T^4}{dy^2} \tag{2}$$

where dp/dx is a pressure gradient in the channel in the flow direction, *i.e.*, x-direction, which is perpendicular to the y-direction (constant everywhere), T = T(y) is the medium temperature, k is the thermal conductivity of the fluid, β is the thermal expansion coefficient, μ is the dynamic viscosity, ρ is the fluid density, and $T_{ref}$ is a constant reference temperature defined as $T_{ref} = (T_L + T_R)/2$. σ is the Stefan-Boltzmann constant and χ is the mean absorption coefficient of the medium. Since the channel size is on a microscale, the velocity slip and the temperature jump need to be considered as the boundary conditions at the solid walls:

$$u\left(y=L\right)=l_v\left(\frac{du}{dy}\right)_{y=L} \tag{3}$$

$$u(y=-L)=l_v\left(\frac{du}{dy}\right)_{y=-L} \tag{4}$$

$$T\,(y=L)=T_R+l_T\left(\frac{dT}{dy}+\frac{4\sigma}{3k\chi}\frac{dT^4}{dy}\right)_{y=L} \tag{5}$$

$$T\,(y=-L)=T_R+l_T\left(\frac{dT}{dy}+\frac{4\sigma}{3k\chi}\frac{dT^4}{dy}\right)_{y=-L} \tag{6}$$

where $l_v$ is the velocity slip length and $l_T$ is the temperature slip length, which is referred to as "temperature jump length" hereafter. From the Maxwell theory for gases the mean free path of the molecules is equal to velocity slip length and can be estimated from the $l=3\mu/2\rho a$ where "a" is the sound speed. Also the temperature slip length from the Maxwell theory is equal to $l_T=\frac{2C_pl_v}{C_p+C_v}\frac{C_p\mu}{k}$. There is no analytical formula for liquids and many experimental studies have been performed [33–39] reporting a wide range of slip lengths, ranging from micrometers to nanometers (including no-slip). Furthermore, molecular dynamics simulations suggest slip lengths of less than 100 nm [33–35], which were confirmed by experiments using near-surface particle tracking [36,37]. Hydrophobic surfaces do appear to introduce a discernible but small slip length of approximately 10–50 nm [38,39]. The modelling of velocity slip and temperature jump at a fluid-solid interface is not easy due to the complexity of the phenomena themselves. However, in this study the simplest models of Equations (3)–(6) are applied, which resemble those for fluid-solid interface, because the purpose of the current study is to investigate the physical essence rather than the quantitative details. Nevertheless, the correct physical principle from the simplest velocity slip and temperature jump models could be extracted even though they could have clear limitation in predicting the accurate quantities.

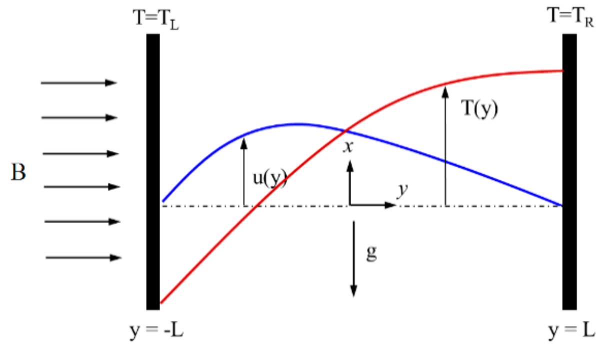


**Figure 2.** Schematic of the system.

In thermodynamics, entropy is a measure of the number of specific ways in which a thermodynamic system may be arranged (a measure of disorder). According to the Second Law of Thermodynamics the entropy of an isolated system never decreases; such a system will spontaneously evolve toward thermodynamic equilibrium, the configuration with maximum entropy. The current channel which is not isolated and has the irreversible processes decrease in entropy provided they increase the entropy of its environment by at least that same amount (increase the combined entropy of the system and its environment). The entropy is a state function and its change related to the initial and final state.

The irreversibility in channel flow of a fluid has two components of energy and momentum. Consequently, entropy production may occur as a result of fluid friction and heat transfer in the direction of finite temperature gradients. Following Bejan [40,41], the volumetric rate of entropy generation can be expressed as:

$$\dot{S}_g''' = \frac{k}{T^2}\left(\frac{dT}{dy}\right)^2 + \frac{\mu}{T}\left(\frac{du}{dy}\right)^2 \tag{7}$$

The first term in Equation (7) describes the heat transfer irreversibility and the second term represents the local entropy generation rate due to fluid friction, respectively. Energy minimization methods [41,42] seek the maximum exergy of a system (the maximum useful work possible during a process that brings the system into equilibrium with a heat reservoir). In the current system the description of the exergy is the potential of the fluid in channel to cause a change as it achieves equilibrium with its wall at constant temperature. In the present system, exergy is destroyed because the process involves a temperature change. This destruction is proportional to the entropy increase of the system together with its surroundings, so the minimization of the entropy generation is equal to the maximization of the energy that is available to be used in the system.

In order to clarify the physical essence, in this study the non-dimensionalized variables are introduced. The non-dimensional of main variables are:

$$X = \frac{x}{L} \tag{8}$$

$$Y = \frac{y}{L} \tag{9}$$

$$U(Y) = \frac{u(y)}{u_m} \tag{10}$$

$$\theta(Y) = \frac{T - (T_L + T_R)/2}{T_R - T_L} \tag{11}$$

$$P = \frac{pL}{\mu u_m} \tag{12}$$

and the non-dimensional parameters which arise are:

$$Gr = \frac{g\beta(T_R - T_L)L^3}{2\nu^2} \tag{13}$$

$$\mathrm{Re} = \frac{u_m L}{\nu} \tag{14}$$

$$R_d = \frac{\sigma(T_R - T_L)^3}{3k\chi} \tag{15}$$

$$\theta_R = \frac{(T_L + T_R)/2}{T_R - T_L} \tag{16}$$

$$Ha = BL\sqrt{\frac{\sigma}{\mu}} \tag{17}$$

$$\lambda_v = \frac{l_v}{L} \tag{18}$$

$$\lambda_T = \frac{l_T}{L} \tag{19}$$

$$N_s = \frac{L^2 \dot{S}_g'''}{k} \tag{20}$$

$$Br = \frac{\mu}{k(T_R - T_L)}(u_m)^2 \tag{21}$$

$$Be = \frac{\left(\frac{d\theta}{dY}\right)^2}{\left(\frac{d\theta}{dY}\right)^2 + Br\left(\frac{dU}{dY}\right)^2} \tag{22}$$

where the Gr is the Grashof number, Re is the Reynolds number, $R_d$ is the radiation parameter, Ha is the Hartmann number (the ratio of electromagnetic force to the viscous force in the absence of the Hall effect, electrical and polarization effects), and $\theta_R$ is the temperature parameter, Be is the Bejan number (in the context of thermodynamics,the ratio of heat transfer irreversibility to total irreversibility due to heat transfer and fluid friction; in the context of fluid mechanics, the dimensionless pressure drop along a channel), Br is the ratio between heat produced by viscous dissipation and heat transported by molecular conduction (the ratio of viscous heat generation to external heating), and $N_s$ is the dimensionless form of local entropy generation rate in Equation (7). From Equation (22), it is obvious that the Bejan number ranges from 0 < Be < 1. While Be = 0 represents the limit case of fluid friction dominated irreversibility, Be = 1 corresponds to the limit case of heat transfer dominated irreversibility. The contribution of both heat transfer and fluid friction to entropy production in the flow system is the same when Be = 0.5.

As the term $u_m = \frac{1}{2}\int_{-L}^{L} u(y)\,dy$ is a constant ($\int_{-1}^{1} U(Y)\,dY = 2$ can be used to find the pressure gradient). Then, by multiplying Equation (1) in $L^2/u_m$ and Equation (2) in $2L^2/(T_R - T_L)$, respectively, and considering dimensionless parameters in (7)–(18), the non-dimensional momentum and energy equations as a system of ordinary coupled differential equations can be rewritten as:

$$\frac{d^2U}{dY^2} = Ha^2 U - \frac{Gr\theta}{\mathrm{Re}} + \frac{dP}{dX} \tag{23}$$

$$\frac{d^2}{dY^2}\left[\theta + R_d(\theta + \theta_R)^4\right] = 0 \tag{24}$$

In addition, the non-dimensional form of the boundary conditions in the equations from (3) to (6) can be rewritten as:

$$U(Y=1)=\lambda_v\left(\frac{dU}{dY}\right)_{Y=1} \tag{25}$$

$$U(Y=-1)=\lambda_v\left(\frac{dU}{dY}\right)_{Y=-1} \tag{26}$$

$$\theta(Y=1)=1+\lambda_T\frac{d}{dY}\left[\theta+R_d(\theta+\theta_R)^4\right]_{Y=1} \tag{27}$$

$$\theta(Y=-1)=-1+\lambda_T\frac{d}{dY}\left[\theta+R_d(\theta+\theta_R)^4\right]_{Y=-1} \tag{28}$$

The components of dimensionless entropy generation are:

$$S_U=\frac{1}{(\theta+\theta_R)}\left(\frac{dU}{dY}\right)^2 \tag{29}$$

$$S_\theta=\frac{1}{(\theta+\theta_R)^2}\left(\frac{d\theta}{dY}\right)^2 \tag{30}$$

## 3. Results and Discussion

The problem of optimal design of a steady state mixed convection MHD flow in a vertical channel filled with radiative absorbing medium is solved under the no-slip and slip-flow conditions at the channel walls in the presence of a crosswise uniform magnetic field. The Newtonian, incompressible and electrically conducting fluid is assumed. With the aim of acquiring a comprehensive vision of the physical problem, estimations have been accomplished to get the flow and temperature field with Hartmann number (Ha), radiation parameter ($R_d$), mixed convection parameter (Gr/Re), thermal parameter ($\theta_R$), temperature jump ($\lambda_T$), and velocity slip ($\lambda_v$) asshown in Figures 3–8. The non-dimensional governing Equations (23)–(28) are solved numerically using Runge–Kutta–Fehlberg method [52] with shooting technique [53]. The set of simultaneous first order differential equations of equivalent initial-value problem ($Z' = f(Z,Y)$) are constructed by the vector $Z = [U\ U'\ \theta\ \theta']$ and the first guess of the initial value is assumed as $Z(Y = -1) = [0\ 0\ -1\ 0]$.

Figure 3 presents the effect of thermal radiation parameter on the various aspect of thermal and fluid flow of the system for the Grashof number to Reynolds number ratio of one hundred, and $\lambda_T = 0.01$, $\lambda_v = 0.01$, $\theta_R = 10$, Ha = 0.1. For the case of no the thermal radiation effect ($R_d = 0$), the temperature profile is linear ($\theta = Y$). By increasing the thermal radiation coefficient from $10^{-4}$ to $10^{-2}$ the dimensionless temperature gradient increased, especially near the left wall as shown in Figure 3a, which leads to an increase of the heat transfer component of the entropy. Figure 3b shows the wavy shape of the velocity component of the entropy profile. By increasing the thermal radiation coefficient, the dimensionless velocity profile becomes flattened. The minimum velocity component of the entropy value occurs at the peak value of the velocity or zero shear stress points. Furthermore, the maximum velocity component of the entropy value occurs at the walls. The effects of thermal radiation on the total heat transfer and viscous parts of the entropy are illustrated in Figure 3c,d, respectively. By increasing $R_d$, the heat transfer part of the entropy increases dramatically while the viscous part of the entropy decreases.

Although the entropy generation due to thermal effects increases, it is two orders of magnitude ($10^{-1}$ *vs.* $10^{1}$) smaller with respect to entropy generated by frictional effects.

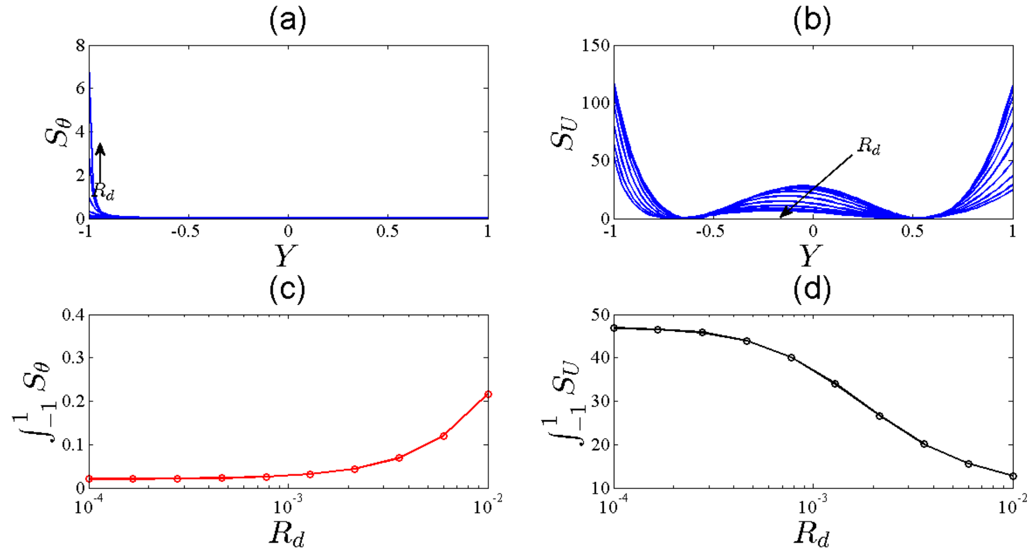


**Figure 3.** Thermal radiation effect on: (**a**) the dimensionless heat transfer component of the entropy; (**b**) the dimensionless viscous component of the entropy; (**c**) the total dimensionless heat transfer component of the entropy; (**d**) the total dimensionless viscous component of the entropy.

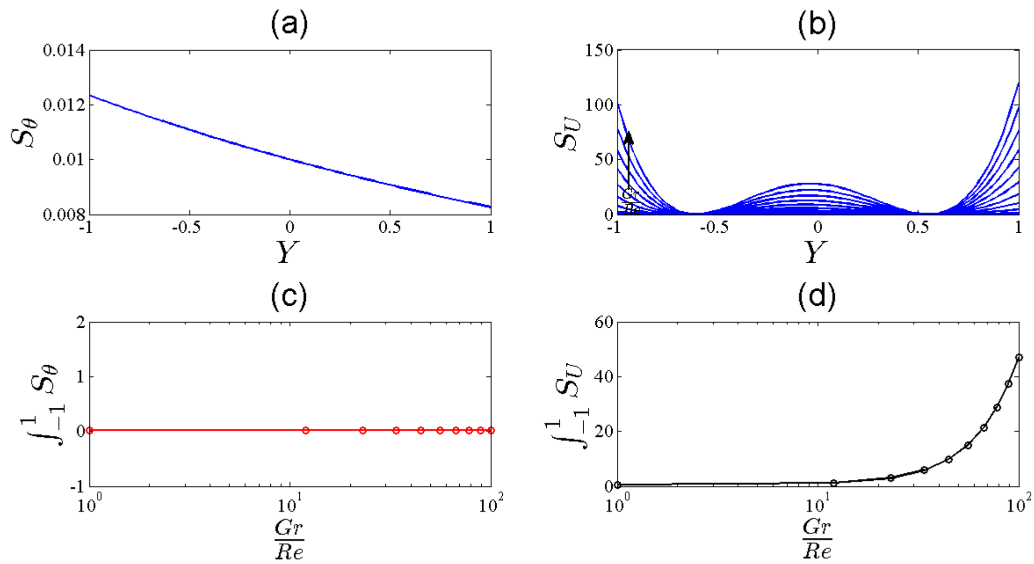


**Figure 4.** Grashof number to Reynolds number ratio effect on: (**a**) the dimensionless heat transfer component of the entropy; (**b**) the dimensionless viscous component of the entropy; (**c**) the total dimensionless heat transfer component of the entropy; (**d**) the total dimensionless viscous component of the entropy.

The effect of the Gr/Re parameter is demonstrated for the $R_d = 10$, and $\lambda_T = 0.01$, $\lambda_v = 0.01$, $\theta_R = 10$, Ha = 0.1 in Figure 4. As seen in Figure 4a, by increasing the Gr/Re from 1 to 30 the $S_\theta$ is constant because the dimensionless temperature is not changed. As shown the $S_\theta$ is maximum at the left wall and decreases smoothly to the right wall. Figure 4b illustrates the influence of the mixed convection parameter Gr/Re, on the dimensionless velocity component of the entropy profiles. As seen by increasing Gr/Re the velocity component of the entropy increases. The maximum again appears at the walls. By increasing of Gr/Re, the dimensionless velocity profile maximum increases. As illustrated in Figure 4c the Gr/Re has no effect on total $S_\theta$, but $S_u$ is increased by increases of Gr/Re (see Figure 4d), so a lower Gr/Re is better from the Second Law of Thermodynamics perspective.

The effect of the Hartmann number is demonstrated in Figure 5. As seen in Figure 5a, by increasing Ha from 5 to 15 for the $R_d$ = 10, $\lambda_T$ = 0.01, $\lambda_v$ = 0.01, $\theta_R$ = 10, and Gr/Re = 50, because the dimensionless temperature profile is not dependent on the Hartmann number the $S_\theta$ not changed. As seen the $S_\theta(Y)$ is approximately linear and has a higher value at the left wall and a lower value at the right wall. Figure 5b shows the distribution of $S_u$ caused by the presence of the magnetic field.

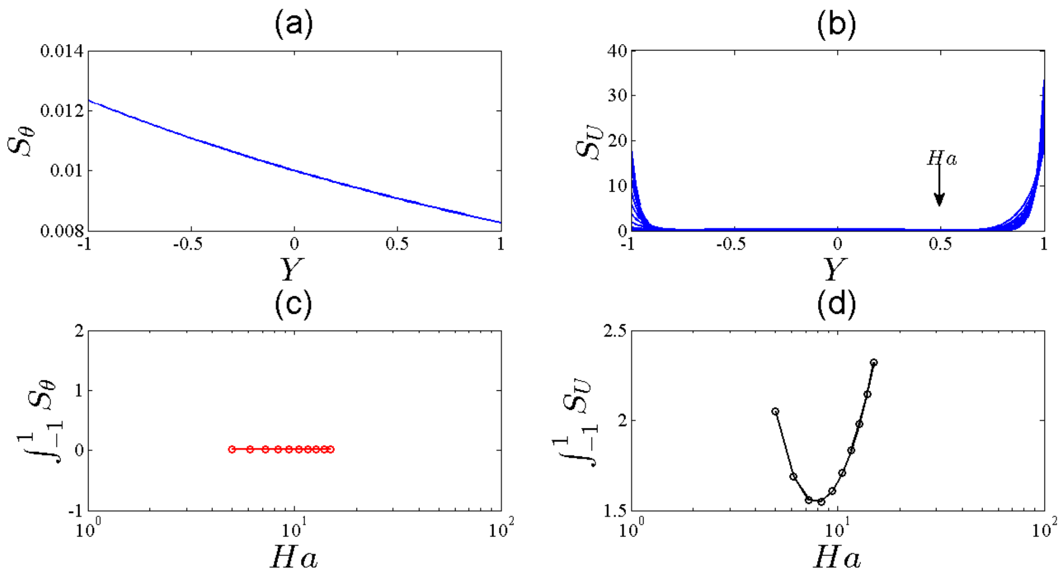


**Figure 5.** Hartmann number effect on: (**a**) the dimensionless heat transfer component of the entropy, (**b**) the dimensionless viscous component of the entropy, (**c**) the total dimensionless heat transfer component of the entropy, (**d**) the total dimensionless viscous component of the entropy.

The existence of the magnetic field generates a resistive force akin to the drag force that acts in the opposite direction of the fluid motion, thus making the velocity of the fluid decrease. By increasing the Hartmann number, the peaks of the dimensionless velocity profile are chamfered so the velocity gradient inside the channel is decreased which leads to lower viscous heating, so the general effect of the magnetic parameter is to decrease the velocity component of the entropy generation. The effect of the Hartmann number on the total $S_\theta$ is exemplified in Figure 5c. As stated before the Hartmann number has no effect on the total $S_\theta$, but as there is a minimum on $S_u$, for the total entropy generation there is a minimum at Ha = 8.

The effect of the thermal parameter is demonstrated for the $R_d$ = 0.01, Gr/Re = 100, $\lambda_T$ = 0.01, $\lambda_v$ = 0.01, and Ha = 0.1 in Figure 6. As shown in Figure 6a by increasing $\theta_R$ from 5 to 9 the dimensionless heat transfer entropy generation is increased, especially near the left wall. Figure 6b shows the wavy shape of the velocity entropy generation component which has a critical point inside and two peaks at the boundaries. As observed, by the increase of $\theta_R$, the dimensionless entropy generation component velocity profile decreases. The effect of $\theta_R$ on the total heat transfer entropy generation is illustrated in Figure 6c. By increasing $\theta_R$, the total heat transfer entropy generation has a parabolic shape with a minimum at $\theta_R = 6.6$. Also the total viscous entropy generation decreases with the increase of $\theta_R$ (see Figure 6d).

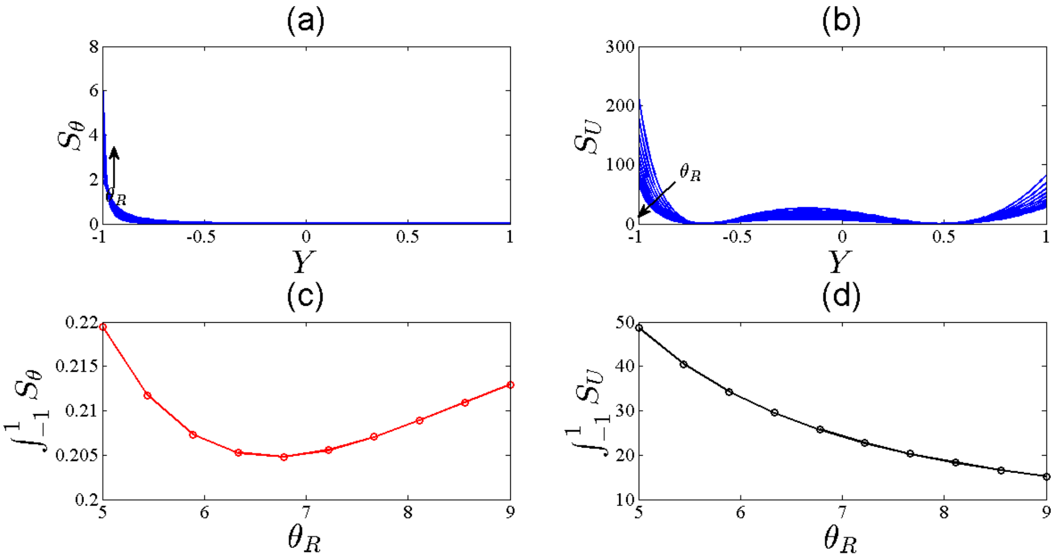


**Figure 6.** Thermal parameter effect on: (**a**) the dimensionless heat transfer component of the entropy; (**b**) the dimensionless viscous component of the entropy; (**c**) the total dimensionless heat transfer component of the entropy; (**d**) the total dimensionless viscous component of the entropy.

In Figure 6, the major contribution to the total entropy is due to the viscous dissipation and this term always decreases with the temperature parameter. Generally, when both the heat transfer entropy generation and viscous entropy generation are summed and displayed on a single curve, the decrease in the viscous entropy generation is dominant and the minimum does not exist. In Figure 7 both terms are added to show the dominance of the decrease in the viscous entropy generation and that there is no minimum on it.

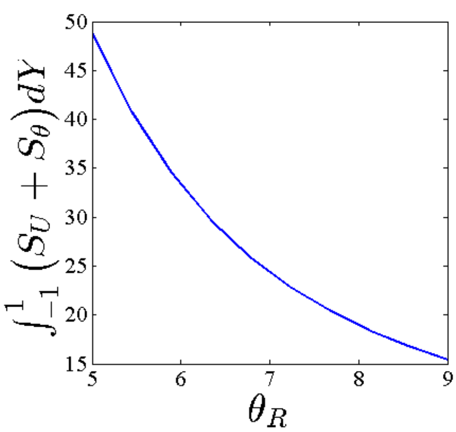


**Figure 7.** Thermal parameter effect on summation of the total dimensionless heat transfer component of the entropy and the total dimensionless viscous component of the entropy.

The effect of velocity slip ratio is demonstrated in Figure 8 by increasing $\lambda_v$ from 0 to 0.05 for the $R_d$ = 0.01, and $\lambda_T$ = 0.01, Ha = 0.1, Gr/Re = 50, $\theta_R$ = 0.1. The $\lambda_v$ is equal to the Knudsen number for gas flow in the channel. It can be noticed from Figure 8a that for different values of $\lambda_v$ the dimensionless heat transfer entropy generation rate is not changed. Further, in Figure 8b it is observed that the viscous entropy generation rate is maximum at the right wall, while the sinus shape of the velocity profile is not altered with an increase of $\lambda_v$. By increasing $\lambda_v$, the maximum dimensionless viscous entropy generation rate profiles increase to some extent. As anticipated from Figure 8a the $\lambda_v$ has no influence on the total dimensionless heat transfer entropy generation rate, while it is clearly seen from these Figure 8d that the total viscous entropy generation rate increases with an increase of $\lambda_v$, so the lower velocity slip is better for maximizing the exergy of the system.

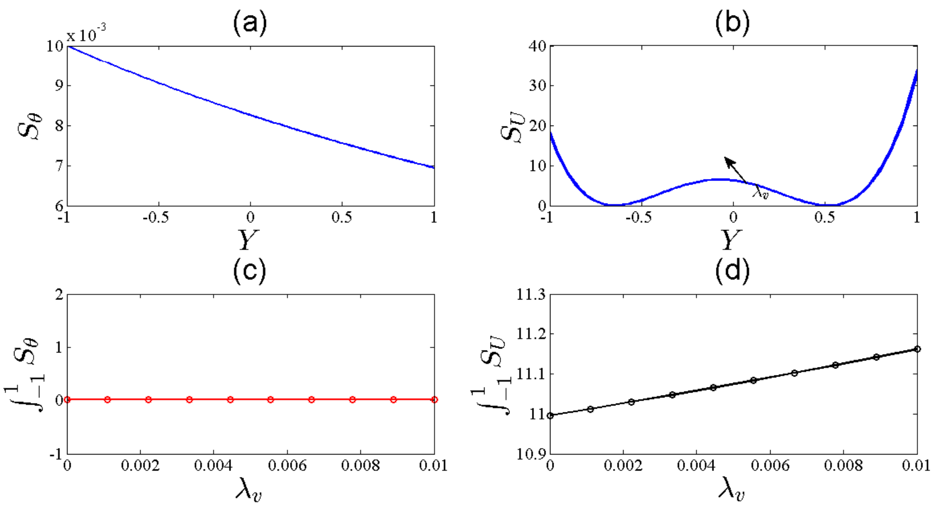


**Figure 8.** Velocity slip effect on: (**a**) the dimensionless heat transfer component of the entropy; (**b**) the dimensionless viscous component of the entropy; (**c**) the total dimensionless heat transfer component of the entropy; (**d**) the total dimensionless viscous component of the entropy

The effect of temperature slip is demonstrated in Figure 9. As depicted in Figure 9a, by increasing $\lambda_T$ from 0 to 0.1 the magnitude of the dimensionless heat transfer entropy generation rate distribution shifted downward. Figure 9b shows the sine-like shape of the velocity entropy generation rate distribution with fixed values of all other parameters as the $R_d$ = 0.01, and $\lambda_v$ = 0.01, Ha = 0.1, Gr/Re = 50, $\theta_R$ = 0.1. By increasing $\lambda_T$, the dimensionless velocity profile is not changed meaningfully, although an increase of $\lambda_T$ causes the increase of $S_u$ at the middle of the channel and a decrease at the left boundary. For the gas flow in a vertical channel the temperature slip is proportional to the velocity slip length ratio or Knudsen number. By increasing of the gas Prantdl number and decreasing the specific heat ratio, the $\lambda_T$ increases. The effect of $\lambda_T$ on the total heat transfer entropy generation rate is illustrated in Figure 9c. By increasing $\lambda_T$, the $S_\theta$ decreases. Furthermore the friction entropy generation rate decreases as $\lambda_T$ increases, as shown in Figure 9d.

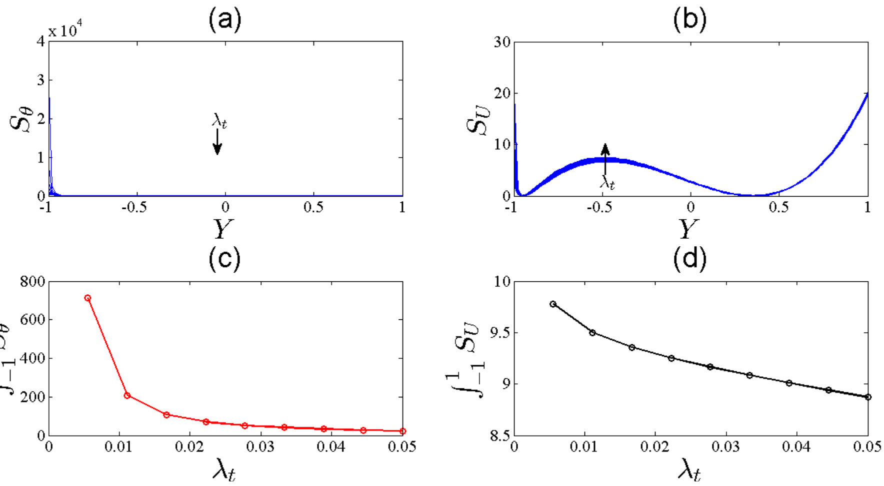


**Figure 9.** Temperature slip effect on: (**a**) the dimensionless heat transfer component of the entropy; (**b**) the dimensionless viscous component of the entropy; (**c**) the total dimensionless heat transfer component of the entropy; (**d**) the total dimensionless viscous component of the entropy

## 4. Conclusions

In this study, the optimization of the steady flow in a filled vertical microchannel with thermal radiation has been thoroughly investigated. The results can be summarized as follows:

(1) By increasing $R_d$, the heat transfer part of the entropy increases dramatically while the viscous part of the entropy decreases.
(2) By increasing $\theta_R$, the total heat transfer entropy generation has a minimum at $\theta_R = 6.6$. Also the total viscous entropy generation decreases as $\theta_R$ increases.
(3) Lower velocity slip, Grashof number to Reynolds number ratio are better for maximize the exergy of the system.
(4) Higher temperature slip is better for maximizing the exergy of the system.
(5) The optimum Hartmann number is about 8.

## Acknowledgments

This research was supported by the Basic Science Research Program through the National Research Foundation of Korea (NRF) funded by the Ministry of Education, Science and Technology (NRF-2012R1A1A1042920).

## Author Contributions

Mohamad Yaghoub Abdollahzadeh Jamalabadi and Jae Hyun Park designed the research with theoretical formulations. Mohamad Yaghoub Abdollahzadeh Jamalabadi performed the numerical simulations. Mohamad Yaghoub Abdollahzadeh Jamalabadi and Jae Hyun Park together analyzed the data and wrote the manuscript for initial submission. Chang Yeop Lee had critical contribution in revising the manuscript including the preparation of responses and English correction. All authors have read and approved the final manuscript.

## Conflicts of Interest

The authors declare no conflict of interest.

## References


1. Barletta, A. Analysis of combine forced and free flow in a vertical channel with viscous dissipation and isothermal-isoflux boundary conditions. *J. Heat Transf.* **1999**, *121*, 349–356.
2. Barletta, A. Fully developed mixed convection and flow reversal in a vertical rectangular duct with uniform wall heat flux. *Int. J. Heat Mass Transf.* **2002**, *45*, 641–654.
3. Boulama, K.; Galanis, N. Analytical solution for fully developed mixed convection between parallel vertical plates with heat and mass transfer. *J. Heat Transf.* **2004**, *126*, 381–388.
4. Modest, M.F. *Radiative Heat Transfer*, 2nd ed.; Academic Press: New York, NY, USA, 2003.
5. Baytaş, A.C.; Liaqat, A.; Groşan, T.; Pop, I. Conjugate natural convection in a square porous cavity. *Heat Mass Transf.* **2001**, *37*, 467–473.
6. Hadjadj, A.; Ben-Nasr, O.; Shadloo, M.S.; Chaudhuri, A. Effect of wall temperature in supersonic turbulent boundary layers: A numerical study. *Int. J. Heat Mass Transf.* **2015**, 81, 426–438.
7. Kandlikar, S.G. High flux heat removal with microchannels—A roadmap of challenges and opportunities. *Heat Transf. Eng*. **2005**, *26*, 5–14.
8. Zhao, C.Y.; Lu, T.J. Analysis of microchannel heat sinks for electronics cooling. *Int. J. Heat Mass Transf.* **2002**, *45*, 4857–4869.
9. Liu, D.; Garimella, S.V. Investigation of liquid flow in microchannels. *J. Thermophys. Heat Transf.* **2004**, *18*, 65–72.
10. Judy, J.; Maynes, D.; Webb, B.W. Characterization of frictional pressure drop for liquid flows through microchannels. *Int. J. Heat Mass Transf.* **2002**, *45*, 3477–3489.
11. Abdollahzadeh Jamalabadi, M.Y. Effect of fuel inject angle on non-premixed combustion of air/methane mixtures in vertical cylinder. *Int. J. Multidiscip. Res. Dev*. **2014**, *1*, Available online: http://allsubjectjournal.com/vol1/issue5/PartA/pdf/13.1.pdf (accessed on 11 February 2015).
12. Kandlikar, S.G.; Schmit, D.; Carrano, A.L.; Taylor, J.B. Characterization of surface roughness effects on pressure drop in microchannels. *Phys. Fluids* **2005**, *17*, doi:10.1063/1.1896985.
13. Abdollahzadeh Jamalabadi, M.Y.; Ghasemi, M.; Hamedi, M.H. Two-dimensional simulation of thermal loading with horizontal heat sources. *Proc. Inst. Mech. Eng. C* **2012**, *226*, 1302–1308.
14. Abdollahzadeh Jamalabadi, M.Y.; Ghasemi, M.; Hamedi, M.H. Numerical investigation of thermal radiation effects on open cavity with discrete heat sources. *Int. J. Numer. Methods Heat Fluid Flow* **2013**, *23*, 649–661.
15. Abdollahzadeh Jamalabadi, M.Y. Experimental investigation of thermal loading of a horizontal thin plate using infrared camera. *J. King Saud Univ. Eng. Sci.* **2014**, *26*, 159–167.
16. Abdollahzadeh Jamalabadi M.Y.; Park, J.H. Thermal radiation, joule heating, and viscous dissipation effects on MHD forced convection flow with uniform surface temperature. *Open J. Fluid Dyn.* **2014**, *4*, 125–132.
17. Abdollahzadeh Jamalabadi, M.Y. Analytical study of Magnetohydrodynamic propulsion stability. *J. Mar. Sci. Appl.* **2014**, *13*, 281–290.

18. Shahidian, A.; Ghassemi, M.; Khorasanizade, S.; Abdollahzade, M.; Ahmadi, G. Flow Analysis of non-Newtonian blood in a magnetohydrodynamic pump. *IEEE Trans. Magn.* **2009**, *45*, 2667–2670.
19. Abdollahzadeh Jamalabadi M.Y.; Park, J.H. Electro-magnetic ship propulsion stability under gusts. *Int. J. Sci. Basic Appl. Res.* **2014**, *1*, 421–427.
20. Abdollahzadeh Jamalabadi, M.Y.; Park J.H.; Lee, C.Y. Thermal radiation effects on the onset of unsteadiness of fluid flow in vertical microchannel filled with highly absorbing medium. *Therm. Sci.* **2014**, doi:10.2298/TSCI140418124A.
21. Field, J.E.; Hahn, K.H.; Harris, S.E.; Observation of electromagnetically induced transparency in collisionally broadened lead vapor. *Phys. Rev. Lett.* **1991**, *67*, 3062–3065.
22. Lemoff, B.E.; Yin, G.Y.; Gordon III, C.L.; Barty, C.P.J.; Harris, S.E. Demonstration of a 10-Hz femtosecond-pulse-driven XUV laser at 41.8 nm in Xe IX. *Phys. Rev. Lett.* **1995**, *74*, 1574–1577.
23. Kadowaki, M.; Yoshizawa, H.; Mori, S.; Suzuki, M. Plasma CVD on the inner surface of a microchannel. *Thin Solid Films* **2006**, *506*, 123–127.
24. Kumar, V.; Paraschivoiu, M.; Nigam K.D.P. Single-phase fluid flow and mixing in microchannels. *Chem. Eng. Sci.* **2011**, *66*, 1329–1373.
25. Aghanajafi, C.; Vandadi, V.; Shahnazari, M.R. Investigation of convection and radiation heat transfer in rhombus microchannels. *Int. J. Res. Rev. App. Sci.* **2010**, *3*, 167–176.
26. Leibrandt, D.R.; Drake, R.P.; Reighard, A.B. A validation test of the flux-limited diffusion approximation for radiation hydrodynamics. *Astrophys. J.* **2005**, *626*, 616–625.
27. Karniadakis, G.; Beskok, A.; Aluru, N. *Microflows and Nanoflows: Fundamentals and Simulation*; Springer: New York, NY, USA, 2003.
28. Ulmanella U.; Ho, C.M. Molecular effects on boundary condition in micro/nanoliquid flows. *Phys. Fluids* **2008**, *20*, doi: 10.1063/1.3006031.
29. Bocquet, L.; Barrat, J.-L. Flow boundary conditions from nano- to micro-scales. *Soft Matt.* **2007**, *3*, 685–693.
30. Horvath, J.A.; Webb, R.N. Experimental study of radiation absorption by microchannels of varying aspect ratios. *Solar Energ.* **2011**, *85*, 1035–1040.
31. Hossain, M.S.;Saidur, R.; Fayaz, H.; Rahim, N.A.; Islam, M.R.; Ahamed, J.U.; Rahman, M.M. Review on solar water heater collector and thermal energy performance of circulating pipe. *Renew. Sustain. Energ. Rev.* **2011**, *15*, 3801–3812.
32. Taylor, R.A.; Phelan, P.E.; Otanicar, T.P.; Adrian. R.; Prasher, R. Nanofluid optical property characterization: towards efficient direct absorption solar collectors. *Nanoscale Res. Lett.* **2011**, *6*, doi:10.1186/1556-276X-6-225.
33. Thompson, P.A.; Troian S.M. A general boundary condition for liquid flow at solid surfaces. *Nature* **1997**, *389*, 360–362.
34. Barrat, J.-L.; Bocquet L. Large slip effect at a nonwetting fluid-solid interface. *Phys. Rev. Lett.* **1999**, *82*, 4671–4674.
35. Cieplak, M.; Koplik J.; Banavar J.R. Boundary conditions at a fluid-solid surface. *Phys. Rev. Lett.* **2001**, *86*, 803–806.
36. Guasto, J.S.; Breuer K.S. High-speed quantum dot tracking and velocimetry using evanescent wave illumination. *Exp. Fluids* **2009**, *47*, 1059–1066.

37. Bouzigues, C.I.; Tabeling, P.; Bocquet L. Nanofluidics in the Debye layer at hydrophilic and hydrophobic surfaces. *Phys. Rev. Lett.* **2008**, *101*, doi:10.1103/PhysRevLett.101.114503.
38. Huang, P.; Guasto, J.S.; Breuer, K.S. Direct measurement of slip velocities using three-dimensional total internal reflection velocimetry. *J. Fluid Mech*. **2006**, *566*, 447–464.
39. Huang, P.; Breuer, K.S. Direct measurement of slip length in electrolyte solutions. *Phys. Fluids* **2007**, *19*, doi:10.1063/1.2539829.
40. Bejan, A. Second-law analysis in heat transfer and thermal design. *Adv. Heat Transfer* **1982**, *15*, 1–58.
41. Bejan, A. *Entropy Generation Minimization*; CRC: Boca Raton, FL, USA, 1996.
42. Makinde, O.D.; Eegunjobi, A.S. Entropy generation in a couple stress fluid flow through a vertical channel filled with saturated porous media. *Entropy* **2013**, *15*, 4589–4606.
43. Eegunjobi, A.S.; Makinde, O.D. Combined effect of buoyancy force and Navier slip on entropy generation in a vertical porous channel. *Entropy* **2012**, *14*, 1028–1044.
44. Ozkol, I.; Komurgoz, G.; Arikoglu, A. Entropy generation in the laminar natural convection from a constant temperature vertical plate in an infinite fluid. *J. Power Energ.* **2007**, *221*, 609–616.
45. Mahmud, S.; Fraser, R.A. Mixed convection-radiation interaction in a vertical porous channel: Entropy generation. *Energy* **2003**, *28*, 1557–1577.
46. Tasnim, S.H.; Shohel, M.; Mamum, M.A.H. Entropy generation in a porous channel with hydromagetic effect. *Exergy: Int. J.* **2002**, *2*, 300–308.
47. Chauhan, D.S.; Kumar, V. Heat transfer and entropy generation during compressible fluid flow in a channel partially filled with porous medium. *Int. J. Energ. Tech.* **2011**, Available online: http://www.as-se.org/ijet/paperInfo.aspx?ID=19088 (accessed on 13 February 2015).
48. Chen, S.; Liu, Z.H.; Bao, S.; Zheng, C.G. Natural convection and entropy generation in a vertically concentric annular space. *Int. J. Therm. Sci*. **2010**, *49*, 2439–2452.
49. Chen, S. Entropy generation of double-diffusive convection in the presence of rotation. *Appl. Math. Comput.* **2011**, *217*, 8575–8597.
50. Bianco, V.; Manca, O.; Nardini, S. Second law analysis of $Al_2O_3$-water nanofluid turbulent forced convection in a circular cross section tube with constant wall temperature. *Adv. Mech. Eng.* **2013**, *2013*, doi:10.1155/2013/920278.
51. Bianco, V.; Manca, O.; Nardini, S. Entropy generation analysis of turbulent convection flow of $Al_2O_3$–water nanofluid in a circular tube subjected to constant wall heat flux. *Energ. Conver. Manage.* **2014**, *77*, 306–314.
52. Hairer, E.; Nørsett, S.; Wanner, G. *Solving Ordinary Differential Equations I: Nonstiff Problems*; Springer: Berlin/Heidelberg, Germany, 1993.
53. Press, W.H.; Teukolsky, S.A.; Vetterling, W.T.; Flannery, B.P. *Numerical Recipes: The Art of Scientific Computing*; Cambridge University Press, New York, NY, USA, 2007.